STEM-IN-SEM: A RE-EMERGING MATERIAL MEASUREMENT APPROACH*

R. R. KELLER, B. W. CAPLINS, J. D. HOLM
NATIONAL INSTITUTE OF STANDARDS AND TECHNOLOGY
APPLIED CHEMICALS & MATERIALS DIVISION
BOULDER, CO 80305
U. S. A.

BIOGRAPHY

Bob Keller is a Group Leader in the Material Measurement Laboratory at the National Institute of Standards and Technology in Boulder, CO. He holds a B.S. and a Ph.D. in Materials Science and Engineering from the University of Minnesota. He worked as a visiting scientist at the University of Erlangen-Nürnberg in 1991-1992 and the Max-Planck-Institute for Metals Research in 2000-2001. Bob's research interests lie in deformation of materials, failure analysis, material reliability testing & physics, and electron microscopy.

ABSTRACT

Scanning transmission electron microscopy performed in a scanning electron microscope (STEM-in-SEM) is undergoing a striking resurgence. This approach to material measurements provides an attractive complement to higher-energy, higher-resolution transmission electron microscopy (TEM)-based STEM, with strengths stemming from factors such as low energy effects on electron scattering and instrument accessibility. While STEM-in-SEM is indeed re-emerging, its foundations include a history dating to the 1930s. In this contribution, we briefly review that history, the differences in SEM- and TEM-based methodologies due to the order-of-magnitude difference in incident beam energies, and some recent STEM-in-SEM advances enabled by detectors with high angular selectivity.

ACKNOWLEDGEMENTS

We gratefully thank Ryan White and Jake Benzing of NIST for their insightful commentary and assistance in the preparation of this manuscript.

CORRESPONDING AUTHOR DETAILS

Bob Keller

bob.keller@nist.gov

INTRODUCTION

The widespread use of scanning electron microscopy (SEM) for surface studies and routine elemental analysis is well-established, but its use for measuring internal material structure and defects has historically been relatively limited. Recent developments, however, in methodology and hardware as well as applications to a wide range of materials, including those considered to be inefficient scatterers of electrons, have led to not only a "re-discovery" of the use of SEM for characterizing internal structure but also a growing adoption of the approach. Scanning transmission electron microscopy performed in a scanning electron microscope (STEM-in-SEM) is a powerful method in and of itself and when combined in a single facility with transmission electron microscopy (TEM) provides a comprehensive capability for quantitative characterization of almost any substance.

There are several major practical differences associated with SEM-based STEM as compared to the TEM-based approach: (i) Significantly larger specimen chamber. The larger specimen chamber in an SEM affords considerable flexibility in terms of space for accessories such as customized detection systems and apparatus for *in situ* experiments. (ii) Fewer electron optical lenses. An SEM electron optical column typically has a condenser system, scan coils, and an objective lens, with no post-specimen lenses. From an operational perspective, optical alignments are simpler, and there are fewer lens aberrations. For the assumption of elastically scattered electrons, the reciprocity principle suggests that we can treat the SEM-based detected signal as we would the TEM-based source in terms of imaging modalities. In this case, the incident beam convergence angle in TEM corresponds to the detector collection angle in the SEM. For variable collection angles in the SEM, this means that STEM-in-SEM can replicate numerous operational modes in TEM, *e.g.*, phase contrast, diffraction contrast, etc. [1], albeit with some limitations. (iii) Typically, several different detectors available. Transmitted electrons can be captured immediately after exiting a specimen, using any of several different STEM detector technologies. Concurrent signals can usually be collected from a backscattered electron detector and/or a secondary electron detector. Other detection modalities such as specimen current, cathodoluminescence, and electron backscatter diffraction are also readily available, providing several possibilities for enhanced analysis via correlative measurements. (iv) Significantly lower barriers to access. Accessibility is a real-world concern for many organizations. An SEM foundation provides a financially more affordable (roughly one order of magnitude lower cost) route to establishing STEM measurement capabilities. Operational training typically requires less effort for basic operation and alignment than that needed for a TEM-based system. Furthermore, since there is roughly an order of magnitude more SEMs available for each TEM globally, scheduling access is often found to be easier within a single institution.

The foundational concepts for performing measurements by sending a scanned, relatively low energy ($\lessapprox$ 50 keV) electron beam through a material originated with the early work of Manfred von Ardenne, first published in 1938 [2,3]. In that seminal work, a 23 keV beam was transmitted through a ZnO crystal, revealing microstructural detail with a

resolution of approximately 40 nm, in the first demonstration of bright-field STEM imaging. This effort was motivated by the then-newly developed TEM technique. Von Ardenne believed that the resolution of TEM was significantly limited by chromatic aberrations associated with the extensive post-specimen lens system. Because he was involved in the development of television technology at the time, he was also aware of the work of Max Knoll, who demonstrated scanned electron images of surfaces [4]. Von Ardenne thought he could use the control technology of television to make a focused electron beam raster over varying sized regions on the surface of a TEM specimen, without requiring post-specimen lenses to further magnify the effects of scattering out of a single incident beam.

Von Ardenne's first instrument was capable of direct detection of both transmitted (in bright-field and dark-field modalities) and reflected electrons via the use of film. Typical achievable magnifications were in the range of several thousand times as determined by the raster size, and image capture onto film required exposures of the order of 10 to 20 minutes [2]. Over the subsequent couple of years, it became apparent that use of a small objective aperture could lead to further improvements in image quality due to the resulting increased depth of focus. Von Ardenne used this realization to create the first stereo pairs of images in an electron microscope, also performed on ZnO crystals. Though no resolution values are quoted, inspection of these images (*e.g.*, figure 7 in [3], image pair II) suggests the demonstration of a lateral resolution of approximately 4 nm to 5 nm, or one order of magnitude improvement over the initial images from two years earlier.

In this era, numerous further-enabling technological advances also occurred, benefitting both SEM and TEM (see Table I in reference [3]). These included short focal length pole piece lenses, improvements in vibration minimization, development of a secondary electron detector with post-acceleration and photomultiplier, and the first single-field condenser-objective lens. For details on these advances, as well some intriguing historical perspective involving secret work done on the "universal electron microscope" in the late 1930s/early 1940s, see reference [3].

The period from about the second World War to the early 1970s saw some important advances in low-energy STEM imaging. We use this terminology because some instruments in this era resembled our typical views of TEM in terms of column design, including housing the specimen within the high-field region of a condenser-objective lens, but used energies typical of SEMs (in the single to tens of keV range). Of particular note is the work of Albert Crewe and colleagues, who developed in the late 1960s a low-energy STEM instrument with a field emission source and energy filter – it was the first microscope capable of imaging isolated atoms (*i.e.*, not atomic columns) [5]. 1970 saw the introduction of the first electron conversion detector [6], which provided an inexpensive yet effective method for generating signal from transmitted electrons. The principle is simple – transmitted electrons strike a tilted, polished metal surface (Al in their case), generating secondary electrons (SE) that are then collected by a conventional SE detector. The SE signal in this case is modulated by the

intensity of the total transmitted electron yield generated by the incident beam at a particular raster position. These types of detectors remain available today through commercial accessory vendors. Oliver Wells gave a thorough history of SEM methods through the early 1970s, including a section specifically on "transmission SEM" [7].

The period from about 1975 to the early 2000s saw few continued STEM-in-SEM developments beyond those of the pioneers. It also saw relatively little use of the earlier-established techniques. This was primarily because TEMs displayed considerably better image resolution and had the ability to easily generate diffraction data for structure refinement; users saw little need to make SEMs duplicate what the TEM could already do. SEMs had then largely become established as tools to look at topography with occasional compositional analysis. The vendor-led instrumentation advances tended to reflect this – instruments were developed to meet the demand of the users. The cheaper yet still powerful SEM became ubiquitous in many academic and industrial labs, but it developed a reputation for not being a highly sophisticated tool.

However, a resurgence began in the early to mid-2000s, driven by both technological and non- technological factors. Technological factors included the rapid spread of field-emission sources in SEMs and the availability of a variety of STEM-in-SEM holders and detectors. Non-technological factors addressed accessibility, in terms of both lower cost of ownership and simpler operational complexity, as described earlier. Klein et al. produced an excellent review article, summarizing both the technique and applications of STEM-in-SEM through about 2010 [8]. During this time, numerous application interests began arising in materials and samples that were not efficient scatterers of electrons. This was one of the important turning points that started to shift user demands. For example, work on polymers [9], carbon nanotubes [10], and sub-cellular biological structures [11] demanded electron microscopy measurements of structure that both produced strong image contrast and posed less risk of sample damage. The SEM-based approach began to take hold for such substances.

A COMPARISON OF SEM- AND TEM-BASED STEM: ENERGY EFFECTS

The lower beam energies of SEM as compared to TEM became key for those who sought to study specimens that did not scatter electrons efficiently. Figure 1 shows the effects of incident beam energy (E) on elastic scattering cross section (Q) and elastic mean free path (λ) for a scattering angle $\varphi_0 > 2°$ (3.5 mrad), over a beam energy range of 10 keV to 200 keV. A simple classical mechanics treatment of electron-nucleus interactions gives the following for the screened Rutherford elastic scattering cross-section Q [12]:

$$Q(> \varphi_0) = 1.62\ x\ 10^{-20} \frac{Z^2}{E^2} \left(\cot \frac{\varphi_0}{2}\right)^2$$

where Z is atomic number. The associated elastic mean free path λ for electron scattering is given by [12]:

$$\lambda = \frac{A}{N * \rho * Q}$$

where A is atomic weight, N is Avogadro's number, and ρ is density.

Lowering the beam energy by one order of magnitude increases Q by two orders of magnitude, while decreasing λ by two orders of magnitude. These effects imply a significantly greater amount of electron scattering from a given thin sample in SEM-based STEM than in TEM-based STEM. Analogous, though somewhat weaker, energy dependences occur for inelastic scattering, with mean free paths being lower by a factor in the approximate range of four to ten for incident beam energies in the "typical" SEM energy range of 5 keV to 30 keV as compared to a TEM range of 80 keV to 300 keV [13]. Implicit in the increased scattering cross section is the fact that the average scattering angle increases upon decreasing the incident beam energy if one compares the $\cot\frac{\varphi_0}{2}$ term for a constant Q for high versus low energy E.

The lower energy of SEM electrons also reduces the total electron range; however, for typical TEM specimen thicknesses of approximately 100 nm, SEM electron energies are still more than sufficient for significant transmission. For example, the Kanaya-Okayama range, which provides an estimate of the size of the hemispherical interaction volume that contains ≥ 95 % of the electron trajectories associated with both elastic and inelastic scattering, is calculated to be 860 nm in gold for an incident energy of 20 keV [12].

Another prominent effect of the lower beam energy is the fact that the radius of the associated Ewald sphere is significantly smaller than that for typical TEM beam energies. For example, $\frac{1}{wavelength}$ = 11.6 $Å^{-1}$ for 20 keV electrons and 39.9 $Å^{-1}$ for 200 keV electrons, differing by a factor of 3.4. This has two immediate implications for analytical measurements: (i) for a given reflection in a two-beam bright-field image, the deviation parameter increases more rapidly at the lower energy, giving rise to more rapidly changing contrast with distance for defect imaging; this has the effect of producing sharper images of, for example, dislocations [14]. (ii) higher-order Laue zones (HOLZ) are more readily reached in diffraction patterns, providing access to precision lattice parameter measurements in three dimensions. For example, sharp fifth order HOLZ rings in silicon have been observed [15] with a 30 keV incident beam; in that particular work, HOLZ visibility was limited by the phosphor diameter, suggesting detection of yet higher order rings is achievable.

Disadvantages of using a one-order-of-magnitude lower incident beam energy include a higher risk of ionization damage due to the fact that for a given probe current, more electron-specimen interactions occur in a given volume, thereby increasing the chances for ionization events and other energy loss processes. The larger wavelength also suggests that one cannot achieve the same level of lateral spatial resolution as that possible in a higher-energy instrument.

HIGH ANGULAR RESOLUTION STEM-IN-SEM

STEM-in-SEM provides some attractive features for powerful material measurements: extensive electron scattering, large scattering angles, and a large specimen chamber. A STEM detector that collects a significant proportion of the transmitted electron signal, while resolving that signal with high angular resolution, can provide significant benefits to imaging and diffraction.

Reference [15] provides a detailed description of such a detector [16], which we have modified to include a programmable digital micromirror device (DMD) coupled with a photomultiplier tube (PMT) for imaging and an integrating CMOS camera for diffraction. Figure 2 shows a schematic of the detector and associated signal handling hardware. This programmable STEM (p-STEM) detector captures transmitted electrons on a phosphor screen, an image of which is then reflected out of the SEM chamber and focused onto a DMD array, 1024 x 768 pixels in this case. The programmable array can then direct subsets of the image of the scattered signal into either camera, including the simultaneous capture of multiple different subsets. While viewing a full-field diffraction pattern with the CMOS camera, we can program a mask to select micromirrors that are associated with a particular arbitrary subset of scattering angles within that diffraction pattern. Those micromirrors then direct that portion of the transmitted signal falling onto the DMD into the PMT, which is synchronized with the SEM raster, creating a real space image with contrast defined by the masked diffraction pattern conditions. With this arrangement, we have easily replicated collection conditions typically available with commercial STEM detectors: bright-field (BF), annular BF, marginal BF, dark-field (DF), low-angle annular DF, medium-angle annular DF, and high-angle annular DF. A schematic of these imaging modes and their definitions are shown in figure 3.

While the imaging modes shown in figure 3 represent current commercial low-keV STEM detector capabilities, the programmability of the p-STEM approach also allows for much more sophisticated analyses, such as defect characterization by means of imaging with multiple selected diffracted beams. Figure 4 shows two sets of images, with those of 4(a) representing selection of different annular apertures, which collect scattering into integrated angular ranges; these apertures were defined “on the fly” by the operator. Figure 4(b) shows the increased level of detail that can be revealed through selection of, for example, satellite spots as opposed to the broad angular ranges of 4(a). Masking of specific spots is akin to the use of a physical objective aperture, coupled with beam or specimen tilting, for defining imaging conditions in conventional TEM. However, the p-STEM detector allows for definition of multiple specific spots for defining the real-space image, without additional changes to the microscope operating conditions. In fact, the programmability of this system allows for the production of a multiple, arbitrarily shaped apertures, including shapes that are impossible to manufacture. In figure 4b, the satellite reflections represent double diffraction from different populations of nanotwins in a gold foil [17].

This level of angular selectivity is also highly effective for 4D STEM-in-SEM measurements to create, for example, orientation maps over fields of view spanning multiple orders of magnitude [18, 19]. Figure 5 shows such maps from graphene suspended on a commercial TEM grid, covering three orders of magnitude in field of view. The data are estimated to display a range of spatial information content covering nearly six orders of magnitude, from approximately 4 nm to 2 mm, and are related to the coupled effects of raster size and pixel settings. Heterogeneous features that are visible in this particular image series include grain to grain crystallographic orientation, grain boundaries, localized misorientations, and multiple layers. To our knowledge, 4D STEM interrogation of such a wide range of length scales is not readily accessible by other techniques.

SUMMARY AND OUTLOOK

STEM-in-SEM has seen a strong resurgence over the past 10 to 15 years, accompanied by tremendous advances in detection hardware and operational technique for both imaging and diffraction, allowing the development of a STEM method that is a strong complement to established TEM-based STEM methods. The low incident beam energy provides several physics-based advantages for improving information content within data obtained from samples that are relatively inefficient scatterers of electrons, *e.g.*, low-dimensional, low-atomic number substances. The greater scattering cross sections, lower scattering mean free paths, and greater scattering angles lead to transmitted electron signals that are rich in information that can be extracted by taking advantage of the spacious specimen chamber typically available on an SEM platform. STEM detector programmability is easily achieved with off-the-shelf components, allowing for on-the-fly operator definition of arbitrary apertures that can significantly enhance material measurements when synchronized with the SEM beam raster.

While there have been improvements in imaging and diffraction measurement capabilities, there remains a largely unexplored realm of low-energy STEM-in-SEM spectroscopies. There are ventures into low-energy electron energy-loss spectroscopy, and even a commercial spectrometer available, but few studies have addressed the science of how one might take advantage of the dependence of inelastic scattering on primary beam energy. More broadly, in our opinion, there are great opportunities that can benefit from recent advances in large data set generation and handling as well as artificial intelligence and machine learning approaches, with application to, *e.g.*, concurrent correlated data sets involving multi-dimensional information such as spatial position, time, diffraction, elemental composition, and electronic structure.

REFERENCES

1. Crewe, A. V.; High resolution scanning microscopy of biological specimens. Phil. Trans. Roy. Soc. Lond. B 261 (1971), 61-70. https://doi.org/10.1098/rstb.1971.0037.
2. Von Ardenne, M.; Das Elektronen-Rastermikroskop. Z. Phys. 109 (1938) 553-572. https://doi.org/10.1007/BF01341584.

3. Von Ardenne, M; On the History of Scanning Electron Microscopy, of the Electron Microprobe, and of Early Contributions to Transmission Electron Microscopy. Chapter 1 in "The Beginnings of Electron Microscopy," Academic Press, Ed. Peter W. Hawkes (1985) 1-21. https://doi.org/10.1016/B978-0-12-014578-2.50007-2.
4. Knoll, M.; Aufladepotential und Sekundäremission electronenbestrahlter Körper. Z. tech. Phys. 16 (1935) 467-475.
5. Crewe, A. V.; Wall, J.; Langmore, J.; Visibility of Single Atoms. Science 168 (1970) 1338-1340. https://doi.org/10.1126/science.168.3937.1338.
6. Crawford, B. J.; Liley, C. R. W.; A simple transmission stage using the standard collection system in the SEM. J. Phys. E Sci. Instr. 3 (1970) 461-462. http://dx.doi.org/10.1088/0022-3735/3/6/314.
7. Wells, O. C.; "Scanning Electron Microscopy," McGraw-Hill, (1974); section on transmission SEM: pages 8-10. ISBN-13: 978-0-07-069253-4.
8. Klein, T; Buhr, E.; Frase, C. G.; TSEM: A Review of Scanning Electron Microscopy in Transmission Mode and Its Applications. Adv. Imag. Electr. Phys. 171 (2012), 297-356. https://doi.org/10.1016/B978-0-12-394297-5.00006-4.
9. Guise, O.; Stron, C.; Preschilla, N.; Evaluation of STEM-in-SEM vs. TEM for Polymer Applications in an Industrial Setting. Microsc. Microanal. 14(Suppl 2) (2008), 678-679. https://doi.org/10.1017/S1431927608087035.
10. Van Ngo, V.; Hernandez, M.; Roth, B.; Joy, D. C.; STEM Imaging of Lattice Fringes and beyond in a UHR In-Lens Field-Emission SEM. Microsc. Today 15 (2007), 12-17. https://doi.org/10.1017/S1551929500050951.
11. Mendenhall, J. M.; Yorston, J.; Lagarec, K. G.; Bowden, J.; Harris, K. M.; Large volume high resolution imaging of brain neuropil using SEM-based scanning transmission electron microscopy. Program No. 484.17/GG105. 2009 Neuroscience Meeting Planner. Chicago, IL: Society for Neuroscience, 2009. Online.
12. Goldstein, J. I.; Newbury, D. E.; Michael, J. R.; Ritchie, N. W. M.; Scott, J. H. J.; Joy, D. C.; "Scanning Electron Microscopy and X-Ray Microanalysis," 4th Ed., Springer, (2018); section on electron beam-specimen interactions: pp. 2-14. E-book ISBN: 78-1-4939-6676-9. https://doi.org/10.1007/978-1-4939-6676-9.
13. Egerton, R. F.; "Electron Energy-Loss Spectroscopy in the Electron Microscope," 3rd Ed., Springer, (2011); section on physics of electron scattering, pp. 111-229. E-book ISBN: 978-1-4419-9583-4. https://doi.org/10.1007/978-1-4419-9583-4.
14. Callahan, P. G.; Stinville, J. -C.; Yao, E. R.; Echlin, M. P.; Titus, M. S.; De Graef, M.; Gianola, D. S.; Pollock, T. M.; Transmission scanning electron microscopy: Defect observations and image simulations. Ultramicrosc. 186 (2018), 49-61. https://doi.org/10.1016/j.ultramic.2017.11.004.
15. Caplins, B. W.; Holm, J. D.; Keller, R. R.; Transmission imaging with a programmable detector in a scanning electron microscope. Ultramicrosc. 196 (2019), 40-48. https://doi.org/10.1016/j.ultramic.2018.09.006.
16. Jacobson, B. T.; Gavryushkin, D.; Harrison, M.; Woods, K.; "Angularly sensitive detector for transmission Kikuchi diffraction in a scanning electron microscope," Proc. SPIE 9376, "Emerging Digital Micromirror Device Based Systems and Applications VII," 93760K (March 2015). https://doi.org/10.1117/12.2083520.
17. Holm, J. D.; Caplins, B. W.; "STEM-in-SEM: Introduction to Scanning Transmission Electron Microscopy for Microelectronics Failure Analysis," ASM International (2020); ISBN-13: 978-1-62708-292-1. https://doi.org/10.31399/asm.tb.stemsem.9781627082921.
18. Caplins, B. W.; Holm, J. D.; White, R. M.; Keller, R. R.; Orientation mapping of graphene using 4D STEM-in-SEM. Ultramicros. 219 (2020), 113137. https://doi.org/10.1016/j.ultramic.2020.113137.

19. Caplins, B. W.; Holm, J. D.; Keller, R. R.; A programmable dark-field detector for imaging two-dimensional materials in the scanning electron microscope. Proc. SPIE 10932, “Emerging Digital Micromirror Device Based Systems and Applications XI,” 109320E (March 2019). https://doi.org/10.1117/12.2508694.

FIGURES

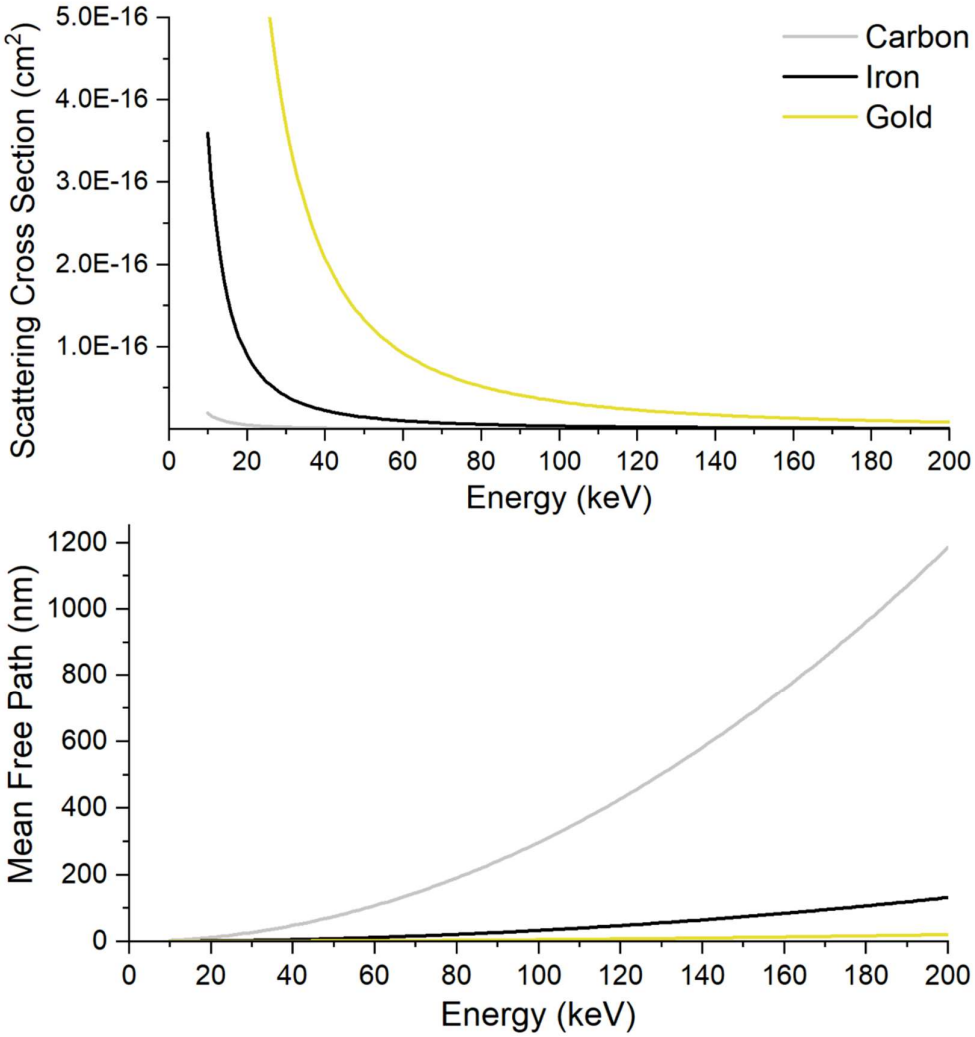

Figure 1. Screened Rutherford elastic scattering cross-section and associated mean free path for C, Fe, and Au over the incident beam energy range 10 keV to 200 keV, for scattering angles more than 2° (3.5 mrad). Lower incident beam energies excel at generating more scattering from smaller volumes.

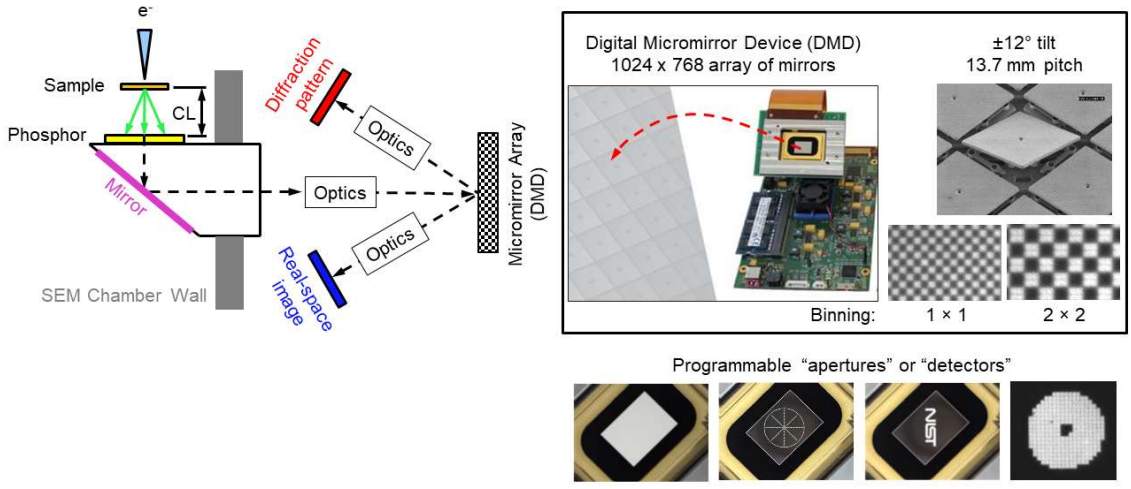

Figure 2. NIST programmable STEM detector based on a digital micromirror device. Transmitted electrons are detected on a phosphor, with an image of the phosphor ported to the DMD device and associated optics, all external to the SEM chamber.

- Bright-Field (BF) – *excludes scattering outside convergence angle*
- Marginal BF (improved image resolution)
- Annular BF (simultaneous high-Z and low-Z elemental contrast)

- Dark-Field (DF) – *excludes straight-through and scattering within convergence angle*
- LAADF (defect contrast enhancement)
- MAADF (grain boundaries, phases, defects)
- HAADF (mass-thickness / Z-contrast)

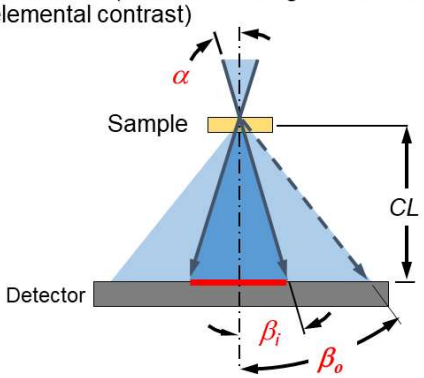

STEM-in-SEM Imaging Mode	Collection Angle Range
Bright-Field (BF)	$\beta_i = 0, \beta_o < \alpha$
Annular Bright-Field (ABF)	$0 < \beta_i, \beta_o < \alpha$
Marginal Bright-Field (MBF)	$\beta_i \approx \alpha$
Dark-Field (DF)	$\alpha < \beta_i$
Low-Angle Annular Dark-Field (LAADF)*	$\beta_i > \alpha$ $\beta_o \leq 50$ mrad
Medium-Angle Annular Dark-Field (MAADF)*	$\beta_i > 50$ mrad $\beta_o < 100$ mrad
High-Angle Annular Dark-Field (HAADF)*	$\beta_i \geq 100$ mrad

*Values are approximate and typical for conventional TEM/STEM instruments.

Figure 3. STEM-in-SEM imaging modes and approximate collection angle conditions.

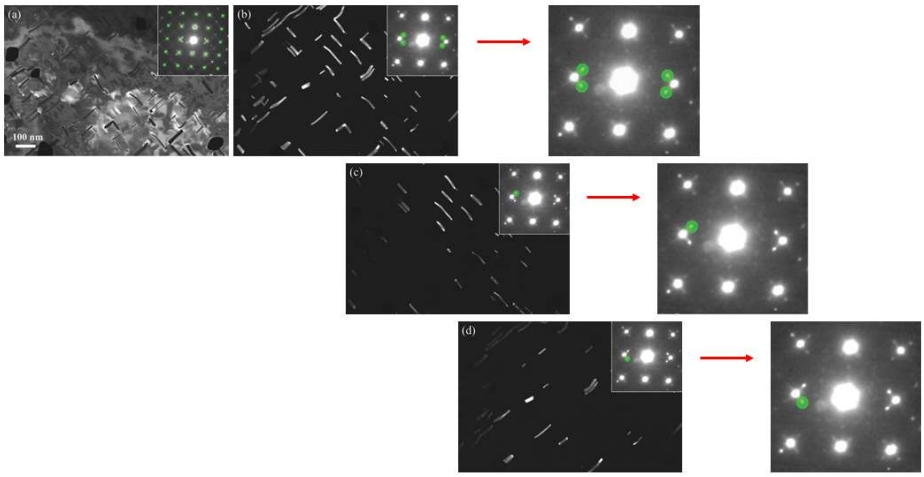

(a)

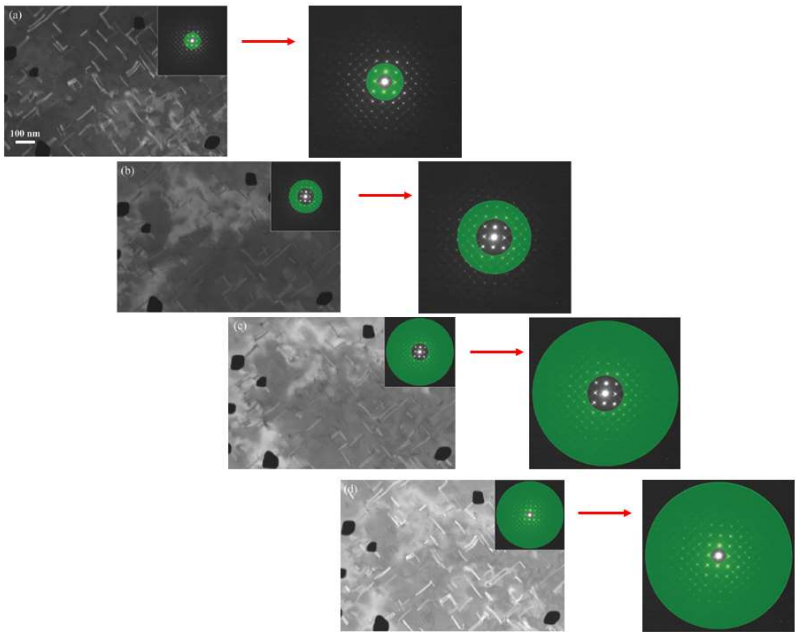

(b)

Figure 4. Effects of the use of different masked regions in the diffraction pattern on defect visibility in a gold foil containing nanotwins. Regions shown in green defined portions of the transmitted signal to be used in image formation. (a) annular selections. (b) direct selection of satellite diffraction spots. Adapted and reprinted from [16] with permission from ASM International.

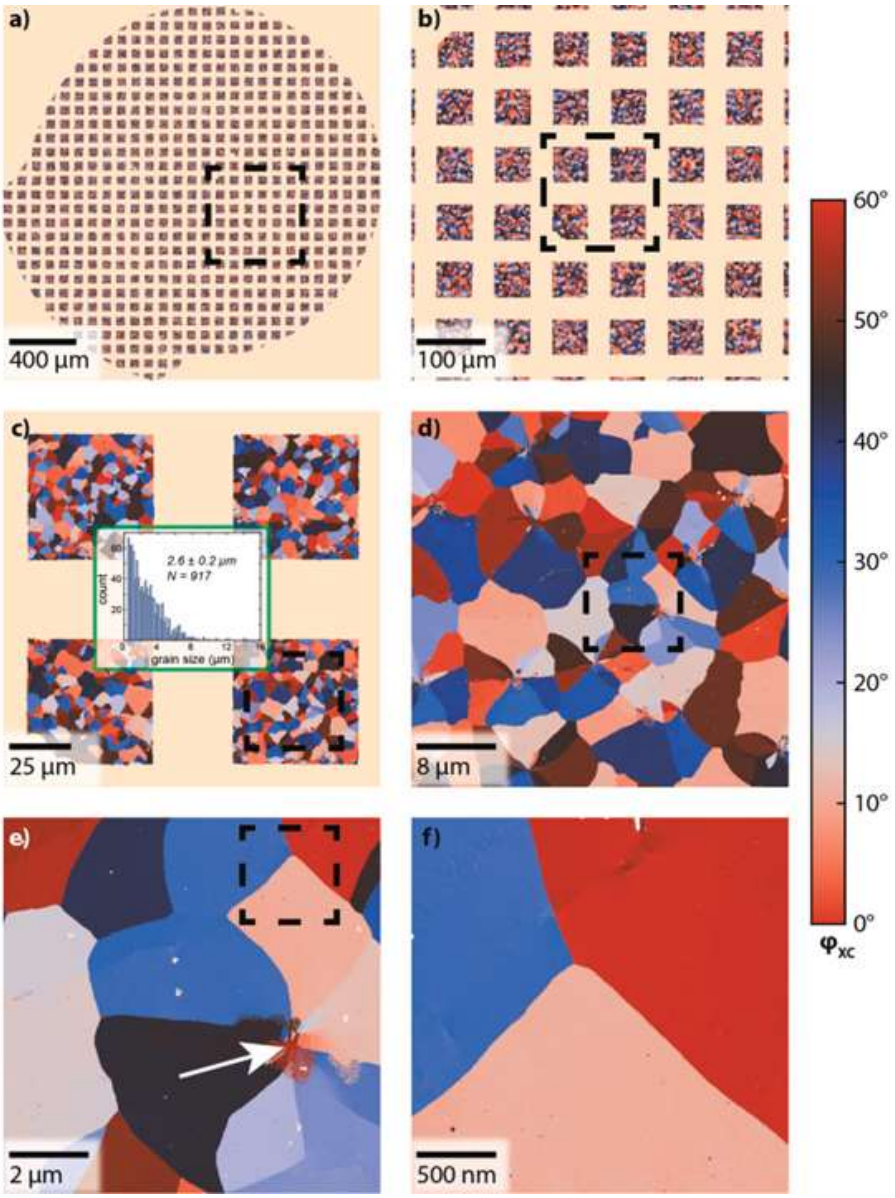

Figure 5. Crystallographic orientation maps of graphene suspended on a commercial TEM grid, which is depicted in beige to represent opacity to electrons. Roughly three orders of magnitude in fields of view are captured in this series, with associated spatial information content spanning nearly six orders of magnitude. Reprinted from [17] with permission from Elsevier.